An Algorithm Differentiating Sunlit and Shaded Leaves for Improving Canopy Conductance and Vapotranspiration Estimates

Li, Jing; Ju, Weimin; He, Wei; Wang, Hengmao; Zhou, Yanlian; Xu, Mingzhu

Published in:
Journal of geophysical research-Biogeosciences

DOI:
10.1029/2018JG004675

JGR Biogeosciences

RESEARCH ARTICLE
10.1029/2018JG004675

Key Points:
- A revised two-leaf light use efficiency model improves gross primary production simulation
- An algorithm differentiating sunlit and shaded leaves for canopy conductance estimate is presented
- Evapotranspiration is substantially improved with canopy conductance estimated using the proposed canopy conductance algorithm

Supporting Information:
- Supporting Information S1

Correspondence to:
W. Ju,
juweimin@nju.edu.cn

Citation:
Li, J., Ju, W., He, W., Wang, H., Zhou, Y., & Xu, M. (2019). An algorithm differentiating sunlit and shaded leaves for improving canopy conductance and evapotranspiration estimates. *Journal of Geophysical Research: Biogeosciences*, *124*, 807–824. https://doi.org/10.1029/2018JG004675

Received 30 JUN 2018
Accepted 26 FEB 2019
Accepted article online 14 MAR 2019
Published online 6 APR 2019

Author Contributions:
Data curation: Yanlian Zhou
Funding acquisition: Weimin Ju
Investigation: Weimin Ju
Writing – review & editing: Weimin Ju, Yanlian Zhou, Mingzhu Xu

An Algorithm Differentiating Sunlit and Shaded Leaves for Improving Canopy Conductance and Vapotranspiration Estimates

Jing Li[1], Weimin Ju[1,2], Wei He[1,3], Hengmao Wang[1], Yanlian Zhou[1], and Mingzhu Xu[1]

[1]International Institute for Earth System Science, Nanjing University, Nanjing, China, [2]Jiangsu Center for Collaborative Innovation in Geographic Information Resource Development and Application, Nanjing, China, [3]Center for Isotope Research, Energy and Sustainability Research Institute Groningen, University of Groningen, Groningen, The Netherlands

Abstract Surface conductance (G_s) is a key parameter in estimating land surface evapotranspiration (ET) and difficult to determine. Here we proposed an approach for determining G_s according to the stomatal conductance of sunlit and shaded leaves that is estimated from their respective gross primary production (GPP) with the Ball-Berry model. Central to this approach, GPP is separately simulated for sunlit and shaded leaves with a revised two-leaf light use efficiency model. We tested the approach at 17 FLUXNET sites with seven different vegetation types. The revised two-leaf light use efficiency model outperforms its predecessor in estimating GPP at most sites. As to G_s estimation, although our proposed algorithm has higher Akaike information criterion values than has the model estimating G_s using vegetation indices, it was able to capture G_s variations at all sites, while models estimating G_s using leaf area index and vegetation indices performed poor at some sites. The proposed algorithm also improves ET estimation, indicated by lower Akaike information criterion, higher determination coefficient (R^2), and lower root mean square error of simulated daily ET for both calibration and validation data sets. This study demonstrates the usefulness of differentiating sunlit and shaded leaves in improving canopy conductance and ET estimates.

1. Introduction

Evapotranspiration (ET) is a key exchange process of mass and energy between the atmosphere and land surface (Chapin et al., 2011; Marshall et al., 2016). It plays a critical role in the terrestrial water cycle, as the land surface returns approximately 60% of precipitation back to the atmosphere at the global scale (Knohl et al., 2003; L'vovich et al., 1990). In parallel with global warming, ET has been enhancing in many regions of the world (Huntington, 2006; Newman et al., 2006). In order to understand the budget and dynamics of the global water cycle, accurate estimation of ET at different spatiotemporal scales becomes seriously crucial (Teuling et al., 2009).

Remote sensing offers an effective and convenient way for estimating ET. It embraces two typical approaches: (i) the vegetation indices (VIs) method, to estimate ET using empirical models driven by VI and meteorological variables (Glenn et al., 2010, 2011; Marshall et al., 2016); and (ii) the energy-balance method, to estimate ET using surface energy balance equations or derived physical models (Allen et al., 2005; Senay et al., 2007). The Penman-Monteith (PM) model is one of such physical models and has been widely applied (Cleugh et al., 2007; Mu et al., 2007; Yebra et al., 2013). It regards the soil-plant-atmosphere continuum as a "big leaf" that exchanges water vapor, momentum, and heat with outside as a whole and integrates the theories of aerodynamics and energy balance (Leuning et al., 2008; Monteith, 1965; Xin et al., 2003). Unlike other models, the PM model does not take land surface temperature or its components as inputs (Leuning et al., 2008) and blends many climate and canopy variables.

Surface conductance (G_s) is a key parameter in the PM model and not directly measurable. It is closely related to leaf area index (LAI), soil moisture, temperature, atmospheric wetness, and leaf physical properties. Yebra et al. (2013) and Mu et al. (2007) realized reasonable estimates of ET using G_s empirically quantified from VIs and LAI, respectively. In vegetation-dominated areas, G_s approximately equals to its major component, the conductance of canopy (G_c; Kelliher et al., 1995). G_c could be used as a proxy of G_s in calculating ET under a dry canopy condition (Irmak et al., 2008; Yebra et al., 2013). Previous studies indicated that G_c could be properly estimated from canopy gross primary production (GPP; Ball et al., 1987; Hu et al., 2009).

Reliable estimation of GPP is a prerequisite for quantifying G_c. Recent studies suggest that differentiation of sunlit and shaded leaves is necessary for improving canopy GPP estimation, since these two groups of leaves have differences in radiation absorption and contributions to canopy carbon assimilation (Norman, 1980; Sinclair et al., 1976). Dai et al. (2004) proposed that the separation of canopy into sunlit and shaded leaves could greatly remedy overestimates of CO_2 and water vapor fluxes. This strategy was also adopted in the Community Land Model 4.0 (Dickinson et al., 2006).

The sunlit and shaded leaves separation approach is also vital for estimating G_s and ET (Irmak et al., 2008; Whitehead et al., 1981). Irmak et al. (2008) empirically estimated G_s as the area-weighted average of the sunlit and shaded leaf stomatal conductance (g_s), which was mainly driven by the photosynthetic photon flux density. Zhang et al. (2011) estimated G_s as the summation of the conductance of sunlit and shaded leaves. The total conductance of sunlit leaves was calculated as the product of g_s per unit of leaf area and total area of these leaves. The total conductance of shaded leaves was calculated through integrating g_s of shaded leaves in different layers within the canopy. For both sunlit and shaded leaves, g_s was quantified using the Jarvis model (Jarvis, 1976). In these studies, g_s of sunlit and shaded leaves was empirically estimated. Uncertainties in estimated g_s would be definitely propagated into G_s estimation.

In this study, we used G_c as a proxy of G_s and proposed a new method for estimating G_s from g_s of the sunlit and shaded leaves, which was determined on the basis of their respective GPP simulated with a revised two-leaf light use efficiency (TL-LUE) model. The estimated G_s was then used to calculate ET, which was validated against measurements at 17 FLUXNET sites with seven different vegetation types. The improvements of our algorithm in calculating G_s and ET over VI-based and LAI-based methods developed by Yebra et al. (2013) and Mu et al. (2007) were also assessed. The objectives of this study are (1) to propose a new method for estimating G_s; (2) to validate the proposed G_s algorithm using G_s derived from tower-based measurements; and (3) to investigate whether the new G_s algorithm can improve the simulation of ET.

2. Data and Methods

2.1. Data

2.1.1. FLUXNET Data

The FLUXNET2015 database (http://fluxnet.fluxdata.org/) provides free data sources for model calibration and validation. We selected 17 sites with data covering at least 6 years (Table 1). At these sites, landscape is relatively homogenous. Around the flux tower at a radius of 1 km, the area proportion of a dominant land cover type is above 50%. The dominant land cover types around these towers include cropland (CRO), deciduous broadleaf forest (DBF), evergreen needleleaf forest (ENF), evergreen broadleaf forest (EBF), grassland (GRA), woody savannas (WS), and savannas (SAV) according to the International Geosphere-Biosphere Programme classification scheme (Hansen & Reed, 2000). Half-hourly observed meteorological data as well as carbon and water fluxes were used in this study. These data were well preprocessed (Moffat et al., 2007; Papale et al., 2006).

Tower-based G_s was derived from observed ET by rearranging the PM equation. We aggregated the half-hour meteorological and flux data in daylight hours to daily values. Daylight hours were decided according to the incoming shortwave radiation (>5 W/m^2; Yebra et al., 2013). In order to reduce the uncertainties in the estimated G_s, days were excluded if there were rainfall in current and previous 2 days. A day without measured data around noon was also excluded. With an assumption that evaporation only accounts for a small fraction, ET can be calculated as follows:

$$\lambda E = \frac{\varepsilon A + \left(\frac{\rho C_P}{\gamma}\right) D G_a}{\varepsilon + 1 + \frac{G_a}{G_s}} \tag{1}$$

where λE (W/m^2) is the latent heat flux, equivalent to ET; G_a (m/s) is the aerodynamic conductance changing with wind speed and vegetation height (Monteith & Unsworth, 2013); $\varepsilon = s/\gamma$, where s (Pa/k) represents the slope of the saturation vapor pressure versus temperature curve and γ (Pa/k) is the

Table 1
Summary of Flux Tower Data Used in This Study

Site ID	Country	Lat.	Lon.	H (m)	Z (m)	IGBP	Area ratio	Reference
US-Ne1	USA	41.17	−96.48	3	6	CRO	0.98	Verma et al. (2005)
US-Ne2	USA	41.16	−96.47	3	6	CRO	0.99	Verma et al. (2005)
US-Ne3	USA	41.18	−96.44	3	6	CRO	0.95	Verma et al. (2005)
DE-Hai	Germany	51.08	10.45	23	44	DBF	0.76	Knohl et al. (2003)
US-MMS	USA	39.32	−86.41	27	48	DBF	0.98	Schmid et al. (2000)
US-WCr	USA	45.81	−90.08	24	30	DBF	0.83	Cook et al. (2004)
AU-Tum	Australia	−35.66	148.15	40	70	EBF	1.00	Leuning et al. (2005)
CA-Qfo	Canada	49.69	−74.34	13.8	24	ENF	0.90	Bergeron et al. (2007)
IT-Lav	Italy	45.96	11.28	33	36	ENF	0.83	Fiora and Cescatti (2006)
NL-Loo	Netherlands	52.17	5.74	15.1	26	ENF	0.71	Dolman et al. (2002)
US-NR1	USA	40.03	−105.55	11.4	21.5	ENF	0.96	Monson et al. (2002)
DE-Gri	Germany	50.95	13.51	1	3	GRA	0.82	Prescher et al. (2010)
US-Var	USA	38.41	−120.95	1	2	GRA	0.60	Ma et al. (2007)
US-Wkg	USA	31.74	−109.94	0.5	6.4	GRA	0.98	Scott (2010)
AU-How	Australia	−12.49	131.15	14	23	SAV	0.50	Beringer et al. (2003)
US-SRM	USA	31.82	−110.87	2.5	6.5	WS	0.93	Scott et al. (2009)
US-Ton	USA	38.43	−120.97	10.1	23.4	WS	0.60	Baldocchi et al. (2010)

Note. Lat. and Lon. denote latitudes and longitudes. H and Z are the heights of canopy and measurement, respectively. Area ratio indicates the area proportion of a dominant land cover type around the flux tower at a radius of 1 km and was determined according to the globeLand30 data sets (Jun et al., 2014). IGBP = International Geosphere-Biosphere Programme; CRO = cropland; DBF = deciduous broadleaf forest; EBF = evergreen broadleaf forest; ENF = evergreen needleleaf forest; GRA = grassland; SAV = savannas; WS = woody savannas.

psychometric constant; $A = Rn - G$, where Rn (W/m^2) is the net absorbed radiation and G (W/m^2) is the soil heat flux; ρ (kg/m^3) is the air density; C_p (J·kg^{-1}·K^{-1}) is the specific heat capacity of air; and D (Pa) is the atmospheric pressure.

Rearranging equation (1), G_s is estimated as follows:

$$G_S = \frac{\lambda E G_a}{\varepsilon A - (\varepsilon + 1)\lambda E + \left(\frac{\rho C_P}{\gamma}\right) D G_a} \tag{2}$$

In equation (1), G_a is calculated as follows:

$$G_a = \frac{k^2 U}{In\left(\frac{z-d}{z_O}\right) In\left(\frac{z-d}{z_{OH}}\right)} \tag{3}$$

where k (= 0.4) is the von Karman constant, U (m/s) is the wind speed at the measurement height (Z, m), d (m) is the zero-plane displacement, Z_O (m) is the aerodynamic roughness corresponding to the wind speed profile, and Z_{OH} (m) corresponding to the temperature profile.

Following Monteith and Unsworth (2013), the last three variables in equation (3) were set as: $d = 2h/3$, $Z_O = 0.123h$, and $Z_{OH} = 0.0123h$, where h (m) is the canopy height (Table 1).

2.1.2. MODIS Data

The C6 version of Moderate Resolution Imaging Spectroradiometer (MODIS) LAI (MCD15A3H) and nadir bidirectional reflectance distribution function (BRDF)-adjusted reflectance (MCD43A4) were used here. The daily 500-m MCD43A4 has been corrected by the BRDF to the nadir direction, which reduced uncertainties in calculated normalized difference vegetation index (NDVI; Rouse et al., 1973), enhanced vegetation index (EVI; Huete et al., 2002), crop factor (*Kc*; Guerschman et al., 2009; Huete et al., 2002), and albedo (Liang, 2001). NDVI, EVI, and *Kc* were smoothed using the locally adjusted cubic-spline capping method (Chen et al., 2006) to remove the unrealistic short-term fluctuations caused by clouds and atmospheric noises. These smoothed variables were used to calculate G_s using the VI-based algorithm proposed by Yebra et al. (2013). The 4-day MODIS LAI was also smoothed using the locally adjusted cubic-spline capping method. And it was temporally interpolated into daily values and used to drive the TL-LUE model and to estimate G_s using the algorithm of Mu et al. (2007).

2.2. G_s Models

2.2.1. The Sunlit-Shaded G_s Model

The Ball-Berry model (Ball et al., 1987) was originally used for estimating g_s according to leaf photosynthesis rate. It has also been used to estimate G_s in vegetated areas (Hu et al., 2009; Luo et al., 2018; Wu et al., 2016). In this study, a G_s model estimating G_s from g_s of the sunlit and shaded leaves was proposed as follows:

$$G_s = g_1 \times \frac{\mathrm{GPP_{shade}} \times h_s}{C_a} + g_2 \times \frac{\mathrm{GPP_{sun}} \times h_s}{C_a} + G_{s,\min} \tag{4}$$

where g_1 and g_2 are the empirical parameters determining the sensitivity of stomatal conductance to photosynthesis rates of sunlit and shaded leaves; $\mathrm{GPP_{sun}}$ and $\mathrm{GPP_{shade}}$ are the photosynthesis rates of sunlit and shaded leaves, respectively; h_s is the relative humidity on canopy surface and assumed equal to the atmospheric one; C_a is the CO_2 concentration in the air; and $G_{s,\min}$ is the surface conductance of soil evaporation and was set to 0.001 for dry conditions in this study.

In equation (4), $\mathrm{GPP_{shade}}$ and $\mathrm{GPP_{sun}}$ are simulated using the revised TL-LUE model. Originally, the TL-LUE model was developed by He et al. (2013) on the basis of the MOD17 algorithm. It separates a canopy into sunlit and shaded leaves. For these two groups of leaves, GPP was individually calculated with the consideration of their differences in light use efficiency and light absorption. Similar to the MOD17 algorithm, the TL-LUE model only captures the stress of low temperature on GPP and ignores the adverse impact of high temperature on carbon fixation by vegetation. In this study, the TL-LUE model was revised by integrating a scalar of temperature borrowed from the Terrestrial Ecosystem Model (TEM) model (Raich et al., 1991), which describes the influences of both low and high temperatures on GPP (equation (9)). The main algorithms in the revised TL-LUE model used to calculate canopy GPP are highlighted as follows (He et al., 2013; Raich et al., 1991):

$$\mathrm{GPP} = \mathrm{GPP_{sun}} + \mathrm{GPP_{shade}} \tag{5}$$

$$\mathrm{GPP_{sun}} = \varepsilon_{\mathrm{msu}} \times \mathrm{APAR_{sun}} \times f(\mathrm{VPD}) \times f(T) \tag{6}$$

$$\mathrm{GPP_{shade}} = \varepsilon_{\mathrm{msh}} \times \mathrm{APAR_{shade}} \times f(\mathrm{VPD}) \times f(T) \tag{7}$$

$$f(\mathrm{VPD}) = \begin{cases} 0 & \mathrm{VPD} \geq \mathrm{VPD_{max}} \\ \dfrac{\mathrm{VPD_{max}} - \mathrm{VPD}}{\mathrm{VPD_{max}} - \mathrm{VPD_{min}}} & \mathrm{VPD_{min}} < \mathrm{VPD} < \mathrm{VPD_{max}} \\ 1 & \mathrm{VPD} \leq \mathrm{VPD_{min}} \end{cases} \tag{8}$$

$$f(T) = \frac{(T - T_{\min})(T - T_{\max})}{(T - T_{\min})(T - T_{\max}) - (T - T_{\mathrm{opt}})^2} \tag{9}$$

where $\varepsilon_{\mathrm{msu}}$ and $\varepsilon_{\mathrm{msh}}$ are the maximum light use efficiency for sunlit and shaded leaves, respectively; $\mathrm{APAR_{sun}}$ and $\mathrm{APAR_{shade}}$ are the absorbed photosynthetically active radiation (APAR) by sunlit and shaded leaves, respectively (Chen et al., 1999); $\mathrm{VPD_{max}}$ and $\mathrm{VPD_{min}}$ are the vapor pressure deficit (VPD) values when GPP achieves the minimum and maximum, respectively, and they were set following Mu et al. (2007); $T_{\max}$, $T_{\min}$, and T_{opt} are the maximum, minimum, and optimal temperatures for photosynthesis, respectively (Raich et al., 1991).

In equation (9), the values of $T_{\min}$ and T_{opt} might be set according to the response of EVI and GPP to the mean daylight air temperature (Wang et al., 2016). In this study, $T_{\min}$ was equal to the average of daylight air temperature where GPP is close to 0 under the low-temperature condition. And this parameter was set to −10 °C when it cannot be determined by GPP. T_{opt} was the maximum turning-point value of the temperature variation curve responded by GPP. $T_{\max}$ was set to 40 °C (Went, 1953). $f(T)$ equals to 0 when the mean daylight air temperature is lower than $T_{\min}$ or higher than $T_{\max}$ (Table 2).

The following equations are used to calculate photosynthetically active radiation (PAR) absorbed by the sunlit and shaded leaves (He et al., 2013):

Table 2
The Parameter Setup of the Revised TL-LUE Model at Each Site

Site ID	IGBP	Ω	T_{opt} (°C)	T_{max} (°C)	T_{min} (°C)	VPD_{max} (kPa)	VPD_{min} (kPa)
US-Ne1	CRO	0.90	32	40	8	4.10	0.93
US-Ne2	CRO	0.90	32	40	8	4.10	0.93
US-Ne3	CRO	0.90	31	40	4	4.10	0.93
DE-Hai	DBF	0.80	19	40	0	4.10	0.93
US-MMS	DBF	0.80	27	40	6	4.10	0.93
US-WCr	DBF	0.80	26	40	2	4.10	0.93
AU-Tum	EBF	0.80	28	40	−10	4.10	0.93
CA-Qfo	ENF	0.60	22	40	−3	4.10	0.93
IT-Lav	ENF	0.60	15	40	−10	4.10	0.93
NL-Loo	ENF	0.60	19	40	−10	4.10	0.93
US-NR1	ENF	0.60	15	40	−4	4.10	0.93
DE-Gri	GRA	0.90	24	40	−4	4.10	0.93
US-Var	GRA	0.90	17	40	−10	4.10	0.93
US-Wkg	GRA	0.90	24	40	−10	4.10	0.93
AU-How	SAV	0.80	31	40	−10	4.10	0.93
US-SRM	WS	0.80	28	40	−2	4.10	0.93
US-Ton	WS	0.80	16	40	−10	4.10	0.93

Note. TL-LUE = two-leaf light use efficiency; IGBP = International Geosphere-Biosphere Programme; CRO = cropland; DBF = deciduous broadleaf forest; EBF = evergreen broadleaf forest; ENF = evergreen needleleaf forest; GRA = grassland; SAV = savannas; WS = woody savannas.

$$\mathrm{APAR_{sun}} = (1-\alpha)\times\left[\mathrm{PAR_{dir}}\times\frac{\cos\beta}{\cos\theta}+\frac{(\mathrm{PAR_{dir}}-\mathrm{PAR_{dif,u}})}{\mathrm{LAI}}+C\right]\times\mathrm{LAI_{sun}} \tag{10}$$

$$\mathrm{APAR_{shade}} = (1-\alpha)\times\left[\frac{(\mathrm{PAR_{dif}}-\mathrm{PAR_{dif,u}})}{\mathrm{LAI}}+C\right]\times\mathrm{LAI_{shade}} \tag{11}$$

$$\mathrm{PAR_{dif}} = \mathrm{PAR}\times\left(0.7527+3.8453\mathrm{R}-16.316R^2+18.962R^3-7.0802R^4\right) \tag{12}$$

$$\mathrm{PAR_{dir}} = \mathrm{PAR}-\mathrm{PAR_{dif}} \tag{13}$$

$$\mathrm{LAI_{sun}} = 2\times\cos\theta\times\left[1-\exp\left(-0.5\times\Omega\times\frac{\mathrm{LAI}}{\cos\theta}\right)\right] \tag{14}$$

$$\mathrm{LAI_{shade}} = \mathrm{LAI}-\mathrm{LAI_{sun}} \tag{15}$$

where α is the canopy albedo and determined according to the MCD43A4 data; $\mathrm{PAR_{dir}}$ and $\mathrm{PAR_{dif}}$ are the direct and diffuse components of incoming PAR, respectively; $\mathrm{PAR_{dif,u}}$ is the diffuse PAR under the canopy; R is the clear-sky index; $\mathrm{LAI_{sun}}$ and $\mathrm{LAI_{shade}}$ are the area indices of sunlit and shaded leaves, respectively; C indicates the contribution of multiple scattering of direct radiation per unit leaf area; β is the leaf angle and was set to 60°; θ is the solar zenith angle; and Ω is the clumping index (Chen et al., 1999; Zhou et al., 2016).

2.2.2. The VI and LAI Based G_s Models

Yebra et al. (2013) proposed an algorithm estimating G_s according to VI:

$$G_s = a\times\exp[b(\mathrm{VI}-\mathrm{VI_{min}})] \tag{16}$$

where a and b are the empirical parameters, VI is the vegetation index and vary with vegetation types, and $\mathrm{VI_{min}}$ is the minimum of VI for bare soils.

In equation (16), VI denotes NDVI for CRO, GRA, WS, and SAV. It is EVI for ENF. As to DBF and EBF, *Kc* is used. The minimum of NDVI, EVI, and *Kc* were set as 0.4, 0.1, and 0, respectively.

Mu et al. (2007) developed a model estimating G_s according to LAI, and this algorithm was employed to generate the MODIS ET product. It is the following:

Table 3
Calibration and Validation Data Sets at All Sites

	Calibration		Validation	
Site ID	Years	Days	Years	Days
US-Ne1	2002, 2003^{n}, 2008^{w}-2009, 2012^{d}	1,094	2004–2005, 2007, 2010–2011, 2013	1,183
US-Ne2	2002, 2003^{n}, 2008^{w}-2009, 2012^{d}	998	2004–2005, 2007, 2010–2011, 2013	1,185
US-Ne3	2002, 2003^{n}, 2008^{w}-2009, 2012^{d}	1,039	2004–2005, 2007, 2010–2011, 2013	1,133
DE-Hai	2003^{d}, 2004^{w}, 2005^{n}	378	2002, 2007–2009	430
US-MMS	2002, 2003^{w}, 2004^{n}, 2005, 2012^{d}	904	2007–2014	1,302
US-WCr	2002, 2003^{n}, 2012^{d}, 2014^{w}	326	2004–2005, 2011, 2013	410
AU-Tum	2003, 2004^{n}, 2007^{d}, 2010^{w}, 2011	1,025	2002, 2005, 2008–2009, 2012–2013	1,213
CA-Qfo	2008^{w}, 2009^{n}, 2010^{d}	324	2004–2005, 2007	383
IT-Lav	2004, 2007^{d}, 2008^{w}, 2009^{n}	566	2010–2014	583
NL-Loo	2005^{d}, 2007^{w}, 2008^{n}	358	2009–2012	397
US-NR1	2009^{n}, 2012^{d}, 2013^{w}, 2014	495	2007–2008, 2010–2011	515
DE-Gri	2012^{n}, 2013^{w}, 2014^{d}	297	2009–2011	281
US-Var	2002, 2003^{n}, 2004, 2011^{w}, 2014^{d}	1,076	2005, 2007–2010, 2012–2013	1,882
US-Wkg	2007^{n}, 2008, 2009^{d}, 2010^{w}	1,237	2004–2005, 2011–2013	1,804
AU-How	2003^{d}, 2010^{n}, 2011^{w}, 2013	682	2007–2008, 2012, 2014	823
US-SRM	2004, 2005^{n}, 2009^{d}, 2010^{w}, 2011	1,527	2007–2008, 2012–2014	1,471
US-Ton	2002, 2003^{n}, 2004, 2011^{w}, 2014^{d}	914	2005, 2007–2009, 2010, 2012–2013	1,646
Total		13,240		16,641

Note. Superscripts n, w, and d denote normal, wet, and dry years, respectively, which were categorized according to monthly air temperature, precipitation, and vapor pressure deficit (supporting information Figures S1–S3). "Days" indicates the number of days with data available for model calibration and validation.

$$G_s = CL \times \mathrm{LAI} \times f(\mathrm{VPD}) \times f(T) + G_{s,\min} \tag{17}$$

where CL is an empirical parameter representing the mean surface conductance per unit LAI, $f(T)$ and $f(\mathrm{VPD})$ are the same as the revised TL-LUE model, and $G_{s,\min}$ is the minimum G_s for soil evaporation and set to 0.001.

For convenience, equations (4), (16), and (17) are named as the SS-G_s, VI-G_s, and LAI-G_s models, respectively, hereinafter. G_s estimated by the SS-G_s, VI-G_s, and LAI-G_s models are named as G_s-SS, G_s-VI and G_s-LAI, respectively. ET estimated using the PM model in conjunction with G_s-SS, G_s-VI, and G_s-LAI are termed as ET-SS, ET-VI, and ET-LAI, respectively.

2.3. Model Calibration and Validation

In order to evaluate the robustness of our model, the calibration data set contains a normal year, a dry year, and a wet year at least. And at most sites, over 50% of the data were selected for validation (Table 3). Tower-based GPP was used to calibrate ε_{msu} and ε_{msh} in the revised TL-LUE model. Tower-based G_s was used to calibrate g_1 and g_2 in the proposed G_s model (equation (4)), a and b in the VI-G_s model (equation (16)), and CL in the LAI-G_s model (equation (17)).

In the calibration process, parameters were allowed to vary at prescribed steps and ranges. The best fit parameter values were determined with the lowest root mean square error (RMSE) of the estimated GPP and G_s against the tower-based values. Both ε_{msu} and ε_{msh} varied in the range from 0 to 12 g C/MJ at a step of 0.1 g C/MJ (Zhou et al., 2016). Both g_1 and g_2 were in a range of 0–60, varying at steps of 1 (Hu et al., 2009). The ranges of a and b were 0–1 mol·m^{-2}·s^{-1} and 0–10, respectively. They varied at steps of 0.01 mol·m^{-2}·s^{-1} and 0.1 (Yebra et al., 2013), respectively. CL ranged from 0 to 1 mol·m^{-2}·s^{-1} with a step of 0.01 mol·m^{-2}·s^{-1} (Mu et al., 2007).

Three accuracy metrics were employed to assess model performances. The coefficient of determination (R^2) and RMSE were used to evaluate the model performances. The Akaike information criterion (AIC) was used to measure the model improvements, and the best model has the lowest AIC value (Inouye et al., 1995). They are calculated as follows:

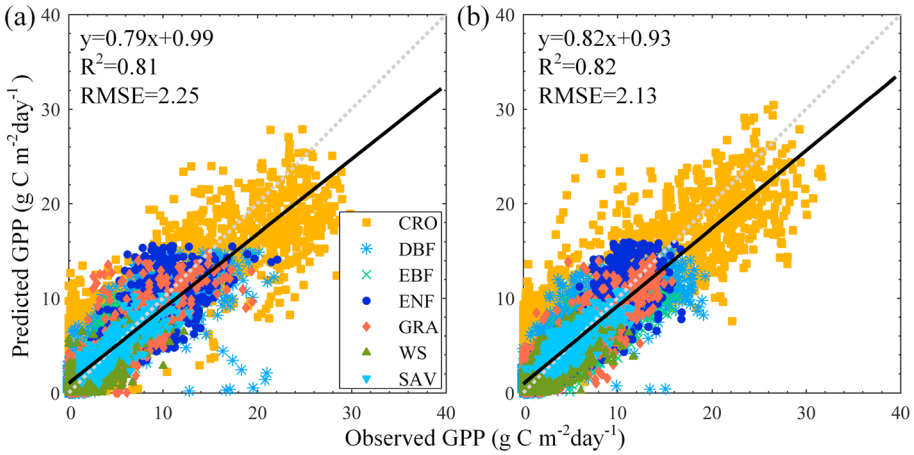

Figure 1. Daily GPP (g C·m^{-2}·day^{-1}) estimated by the revised TL-LUE model: (a) for the calibration data set and (b) for the validation data set. GPP = gross primary production; TL-LUE = two-leaf light use efficiency; RMSE = root mean square error; CRO = cropland; DBF = deciduous broadleaf forest; EBF = evergreen broadleaf forest; ENF = evergreen needleleaf forest; GRA = grassland; SAV = savannas; WS = woody savannas.

$$R^2 = \frac{\sum_{i=1}^{n}(P_i - \overline{O})^2}{\sum_{i=1}^{n}(O_i - \overline{O})^2} \tag{18}$$

$$\mathrm{RMSE} = \sqrt{\frac{1}{n}\sum_{i=1}^{n}(P_i - O_i)^2} \tag{19}$$

$$\mathrm{AIC}(p) = n\ \log E(p) + 2p \tag{20}$$

where P_i is the model-predicted value, O_i is the observed value, $\bar{O}$ is the mean of observed values, n is the number of observations; p is the order of model; and $E(p)$ is the innovation variance (Inouye et al., 1995; Zhou et al., 2016).

3. Results

3.1. Performance of the Revised TL-LUE Model

For the calibration data set, GPP simulated by the revised TL-LUE model agreed well with the tower-based GPP (R^2 = 0.81, RMSE = 2.25 g C·m^{-2}·day^{-1}; Figure 1). For the validation data set, the comparison of daily GPP simulated by the revised TL-LUE model against tower-based GPP produced an R^2 value of 0.82 and an RMSE value of 2.13 g C·m^{-2}·day^{-1} (Figure 1). The validation indicated the revised TL-LUE model was able to capture the variations of the daily GPP in different ecosystems. However, the revised TL-LUE model still tended to underestimate high GPP values slightly (Figure 1).

Figure 2 shows R^2 and RMSE values of daily GPP simulated by the original and revised TL-LUE models against tower-based GPP for both calibration and validation data sets at all sites. The AIC and RMSE values exhibited similar characteristics (Figures 2 and S4). The revised TL-LUE model outperformed the original one at most sites, especially at the CRO, ENF, and GRA sites. At the US-Ne2 (CRO) and US-Var (GRA) sites, the R^2 of daily GPP simulated by the revised model increased by 0.07 and 0.14, respectively, while RMSE decreased by 0.50 and 0.35 g C·m^{-2}·day^{-1}, respectively, and AIC decreased by 501 and 1,232, respectively, in comparison with the corresponding values of the original model.

Table 4 shows the calibrated ε_{msu} and ε_{msh} values for individual sites. Optimal values of ε_{msu} range from 0.4 to 1.6 g C/MJ, and the values of ε_{msh} range from 1.9 to 7.9 g C/MJ. The latter is almost 4 times higher than the former. Zhou et al. (2016) and He et al. (2013) reported that the ε_{msh} parameter was about 3.5–4.8 times of ε_{msu}, which was in accordance with our result. The calibrated values of ε_{msu} and ε_{msh} vary obviously among different land cover types. They are much higher at crop sites than at other sites.

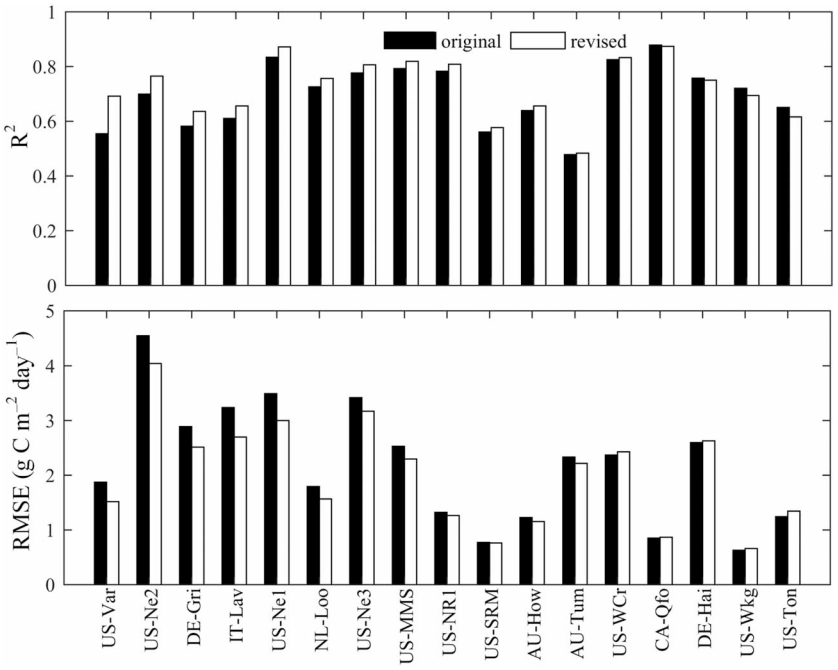

Figure 2. The R^2 and RMSE (g C·m^{-2}·day^{-1}) values of the daily GPP estimated by the original and revised TL-LUE models against the tower-based GPP for both calibration and validation data sets at all sites. Sites were rearranged in the decreasing order of the improvements on R^2 values by the revised TL-LUE model. RMSE = root mean square error; GPP = gross primary production; TL-LUE = two-leaf light use efficiency.

3.2. Calibration and Validation of G_s Models

The calibrated parameters of three G_s models were shown in Table 5. Performances of these models vary with the vegetation types. For the calibration data set, R^2 of G_s-SS against tower-based G_s was higher than that of G_s-VI and G_s-LAI at most sites, with an average increase of 0.06 in R^2. The VI-G_s model had the lowest

Table 4
Calibrated Parameters for the Original and Revised TL-LUE Models

		Revised TL-LUE model					Original TL-LUE model				
Site ID	IGBP	ε_{msh}	ε_{msu}	R^2	RMSE	AIC	ε_{msh}	ε_{msu}	R^2	RMSE	AIC
US-Ne1	CRO	7.9	1.6	0.87	2.99	11,362	6.5	1.3	0.82	3.55	12,051
US-Ne2	CRO	7.9	1.6	0.76	4.11	12,107	6	1.2	0.69	4.62	12,608
US-Ne3	CRO	6.5	1.3	0.80	3.16	11,117	6	1.2	0.77	3.35	11,444
DE-Hai	DBF	2.9	0.6	0.81	2.36	3,802	2.8	0.6	0.81	2.35	3,784
US-MMS	DBF	2.6	0.6	0.76	2.60	9,885	2.4	0.5	0.73	2.79	10,310
US-WCr	DBF	2.4	0.5	0.81	2.40	3,362	2.4	0.5	0.81	2.42	3,326
AU-Tum	EBF	2	0.6	0.45	2.04	9,554	1.6	0.5	0.46	2.04	9,767
CA-Qfo	ENF	2.3	0.5	0.87	0.89	1,802	2.2	0.5	0.87	0.89	1,778
IT-Lav	ENF	3	0.7	0.62	2.82	5,246	2.8	0.8	0.60	3.30	5,643
NL-Loo	ENF	2.4	0.7	0.78	1.47	2,711	2.4	0.7	0.74	1.65	2,909
US-NR1	ENF	2.2	0.5	0.81	1.27	3,286	2	0.6	0.79	1.30	3,374
DE-Gri	GRA	2.2	1	0.59	2.84	2,695	1.7	1.6	0.54	3.19	2,856
US-Var	GRA	1.9	0.4	0.71	1.50	10,819	2.4	0.5	0.56	1.86	12,051
US-Wkg	GRA	3.4	0.7	0.70	0.68	6,095	3.1	0.7	0.73	0.65	5,791
AU-How	SAV	2.7	1	0.71	1.14	4,706	2.8	1	0.68	1.19	4,896
US-SRM	WS	3.9	0.8	0.46	0.79	6,858	3.4	0.7	0.44	0.80	6,976
US-Ton	WS	2.4	0.5	0.66	1.27	8,745	2.4	0.5	0.63	1.31	8,342

Note. All correlations are significant at the level of 0.01. TL-LUE = two-leaf light use efficiency; IGBP = International Geosphere-Biosphere Programme; CRO = cropland; DBF = deciduous broadleaf forest; EBF = evergreen broadleaf forest; ENF = evergreen needleleaf forest; GRA = grassland; SAV = savannas; WS = woody savannas; RMSE = root mean square error; AIC = Akaike information criterion.

Table 5
Calibrated Parameters and Accuracy Metrics of Three G_s Models for the Calibration Data Set

		LAI-G_s				VI-G_s					SS-G_s				
Site ID	IGBP	*CL*	R^2	RMSE	AIC	*a*	*b*	R^2	RMSE	AIC	g_1	g_2	R^2	RMSE	AIC
US-Ne1	CRO	0.36	0.07**	0.46	1,412	0.4	0.9	0.03**	0.39	1,044	15	12	0.07**	0.48	1,480
US-Ne2	CRO	0.41	0.08**	0.45	1,236	0.4	1	0.03**	0.39	942	16	13	0.10**	0.46	1,283
US-Ne3	CRO	0.38	0.12**	0.37	869	0.31	1.84	0.10**	0.32	602	18	14	0.15**	0.37	895
DE-Hai	DBF	0.13	0.04**	0.34	242	0.2	1.31	0.04**	0.27	88	21	14	0.13**	0.30	169
US-MMS	DBF	0.08	0.36**	0.20	−378	0.13	1.68	0.26**	0.19	−422	18	14	0.39**	0.20	−320
US-WCr	DBF	0.13	0.44**	0.28	91	0.04	4.07	0.28**	0.28	95	27	22	0.44**	0.28	106
AU-Tum	EBF	0.15	0.01	0.33	560	0.14	2.21	0.07**	0.27	190	44	9	0.07**	0.29	369
CA-Qfo	ENF	0.14	0.02*	0.29	124	0.26	0.07	0.01	0.22	−72	27	10	0.01	0.29	121
IT-Lav	ENF	0.13	0.06**	0.28	183	0.28	1.37	0.04**	0.23	−27	17	4	0.17**	0.25	35
NL-Loo	ENF	0.14	0.02**	0.28	117	0.4	0.01	0.01	0.26	44	29	6	0.02**	0.29	129
US-NR1	ENF	0.13	0.04**	0.20	−172	0.11	4.38	0.03**	0.17	−323	29	26	0.19**	0.18	−306
DE-Gri	GRA	0.09	0.03**	0.18	−180	0.14	2.03	0.11**	0.12	−413	19	8	0.06**	0.16	−248
US-Var	GRA	0.21	0.34**	0.15	−997	0.07	6.27	0.62**	0.12	−1,554	43	13	0.58**	0.12	−1,477
US-Wkg	GRA	0.2	0.12**	0.06	−3,407	0.1	3.89	0.08**	0.06	−3,458	20	19	0.20**	0.06	−3,388
AU-How	SAV	0.27	0.67**	0.09	−1,346	0.06	7.12	0.77**	0.07	−1,653	19	18	0.65**	0.09	−1,358
US-SRM	WS	0.3	0.17**	0.06	−4,433	0.12	5.34	0.09**	0.06	−4,335	33	32	0.30**	0.05	−4,547
US-Ton	WS	0.16	0.31**	0.12	−1,336	0.07	5.67	0.41**	0.11	−1,506	30	7	0.44**	0.10	−1,535

Note. "LAI-G_s," "VI-G_s," and "SS-G_s" denote G_s models proposed by Mu et al. (2007), Yebra et al. (2013), and this study, respectively. IGBP = International Geosphere-Biosphere Programme; CRO = cropland; DBF = deciduous broadleaf forest; EBF = evergreen broadleaf forest; ENF = evergreen needleleaf forest; GRA = grassland; SAV = savannas; WS = woody savannas; RMSE = root mean square error; AIC = Akaike information criterion.
**Significant at the 0.01 level. *Significant at the 0.05 level.

AIC values at all sites with the exception of the WS site. It performed better than the SS-G_s and LAI-G_s models at the AU-How site (R^2 = 0.77, RMSE = 0.07 mol·m^{-2}·s^{-1}, and AIC = −1,653) and the US-Var site (R^2 = 0.62, RMSE = 0.12 mol·m^{-2}·s^{-1}, and AIC = −1,554).

Table 6 shows accuracy metrics of simulated G_s for the validation data set. Although the proposed SS-G_s model had higher AIC values than had the VI-G_s model, R^2 of G_s-SS was higher than the 0.05 significance level at all sites. The R^2 values of G_s-VI and G_s-LAI were lower than the 0.05 significance level at the DE-Hai and NL-Loo sites, indicating the outperformance of the SS-G_s model over the LAI-G_s and VI-G_s models in capturing daily variations of G_s at different sites. Figure 3 shows the comparison of G_s estimated by three models with tower-based G_s at nine representative sites with different vegetation types. G_s-VI exhibited much smaller seasonal variations in comparison with tower-based G_s at the US-Ne1, CA-Qfo, NL-Loo, DE-Hai, AU-Tum, and IT-Lav sites. The VI-G_s model systematically overestimated low G_s values and underestimated high G_s values at these sites.

The discrepancy between the estimated G_s by three models and the tower-based G_s might be attributed to the following reasons: (1) There are uncertainties in G_s derived from tower-based observations. As not measurable, G_s was derived from tower-based observations of latent heat flux and meteorological data in this study. The uncertainties in tower-based observations and algorithm used to derive G_s would be definitely propagated into estimated G_s. (2) Models assume that G_c can be used as the proxy of G_s, which might be invalid under conditions of low canopy coverage. (3) The LAI-G_s and SS-G_s models estimate G_s according to LAI and GPP, while the tower-based G_s was derived from measured latent heat flux by inverting the PM model. In nongrowing seasons, LAI and GPP were close to 0 at some sites. Accordingly, estimated G_s was very low, close to $G_{s,min}$. However, G_s derived from the tower-based observations might be still high owing to relatively high measured latent heat flux contributed by evaporation from snow on the ground surface and from wet soils.

Calibrated parameters in the LAI-G_s, VI-G_s, and SS-G_s models are shown in Table 5. The values of *CL* in the LAI-G_s model range from 0.08 to 0.41. The values of *a* and *b* in the VI-G_s model range from 0.04 to 0.4 and from 0.01 to 7.12, respectively. The calibrated g_1 and g_2 in the SS-G_s model vary from 15 to 44 and 4 to 32, respectively. The difference between g_1 and g_2 was small for the CRO and SAV sites and large for the EBF and most ENF sites.

Table 6
Accuracy Metrics of Three G_s Models for the Validation Data Set

		LAI-G_s			VI-G_s			SS-G_s		
Site ID	IGBP	R^2	RMSE	AIC	R^2	RMSE	AIC	R^2	RMSE	AIC
US-Ne1	CRO	0.10**	0.47	1,582	0.05**	0.40	1,198	0.10**	0.50	1,697
US-Ne2	CRO	0.04**	0.52	1,796	0.01**	0.45	1,453	0.05**	0.55	1,904
US-Ne3	CRO	0.18**	0.35	855	0.13**	0.31	569	0.17**	0.37	966
DE-Hai	DBF	0.01	0.39	405	0.02**	0.30	183	0.03**	0.36	352
US-MMS	DBF	0.47**	0.15	−1,277	0.35**	0.13	−1,625	0.48**	0.16	−1,097
US-WCr	DBF	0.56**	0.33	262	0.43**	0.36	321	0.51**	0.35	294
AU-Tum	EBF	0.01**	0.32	658	0.03**	0.27	257	0.05**	0.30	518
CA-Qfo	ENF	0.03**	0.31	185	0.01*	0.22	−52	0.01*	0.31	183
IT-Lav	ENF	0.03**	0.31	265	0.02**	0.27	110	0.11**	0.28	160
NL-Loo	ENF	0.02**	0.32	210	0.01	0.29	147	0.10**	0.29	131
US-NR1	ENF	0.02**	0.20	−179	0.05**	0.16	−397	0.14**	0.18	−286
DE-Gri	GRA	0.09**	0.12	−405	0.14**	0.09	−539	0.14**	0.10	−476
US-Var	GRA	0.44**	0.14	−2,138	0.68**	0.10	−3,159	0.63**	0.11	−2,922
US-Wkg	GRA	0.31**	0.05	−5,751	0.23**	0.05	−5,542	0.42**	0.05	−5,826
AU-How	SAV	0.65**	0.09	−1,586	0.70**	0.07	−1,959	0.59**	0.09	−1,613
US-SRM	WS	0.36**	0.05	−4,651	0.25**	0.05	−4,459	0.47**	0.05	−4,480
US-Ton	WS	0.42**	0.10	−2,855	0.51**	0.09	−3,162	0.55**	0.09	−3,266

Note. IGBP = International Geosphere-Biosphere Programme; CRO = cropland; DBF = deciduous broadleaf forest; EBF = evergreen broadleaf forest; ENF = evergreen needleleaf forest; GRA = grassland; SAV = savannas; WS = woody savannas; RMSE = root mean square error; AIC = Akaike information criterion.
**Significant at the 0.01 level. *Significant at the 0.05 level.

3.3. ET Estimation

ET was simulated using the PM model in conjunction with G_s-SS, G_s-VI, and G_s-LAI. The comparison of simulated daily ET against observations indicated that the PM model along with G_s-SS, G_s-VI, and G_s-LAI was able to capture variations of daily ET (Table 7). All three accuracy metrics indicated that the SS-G_s model outperforms the LAI-G_s and VI-G_s models in simulating ET. R^2, RMSE, and AIC of ET-SS against observations averaged 0.75, 0.63 mm/day, and 1,462 for the calibration data set and 0.75, 0.65 mm/day, and 1,842 for the validation data set. The average R^2, RMSE, and AIC of ET-LAI were 0.71, 0.73 mm/day, and 1,621 for the calibration data set and 0.72, 0.74 mm/day, and 2,060 for the validation data set. The corresponding values of ET-VI were 0.65, 0.81 mm/day, and 1,808 for the calibration data set and 0.67, 0.79 mm/day, and 2,229 for the validation data set.

Figure 4 shows the simulated and observed daily ET for the calibration and validation data sets at all sites. Overall, the PM model could accurately simulate the observed daily ET, but it tended to overestimate ET at the CRO, EBF, and ENF sites using G_s-LAI and G_s-VI. The seasonal variations of the simulated and observed daily ET in validation years at the nine representative sites are shown in Figure 5. The PM model was able to capture the seasonality of the observed daily ET. However, it also tended to overestimate high ET in middle growing seasons with G_s-LAI and G_s-VI. The overestimation of ET in middle growing seasons was well remedied with G_s-SS. Similar feature was also observed at the other eight sites (Figure S6).

4. Discussion

4.1. Improvement of the TL-LUE Model

The improvement of the revised TL-LUE model in simulating GPP was achieved by replacing the temperature scalar. In the original model, only the impact of low temperature on GPP is explicitly included, while the impact of high temperature is ignored (Running et al., 2000). As reported by many previous studies (Raich et al., 1991; Wang et al., 2016), both extremely high and low temperatures might restrain photosynthesis. The original model partially accounts for the influence of high temperature through the scalar of VPD. Although high temperature is mostly associated with high VPD, it is not always the case. Thus, the original model might overestimate GPP under high temperature. Integrating a scalar of temperature as used in the TEM

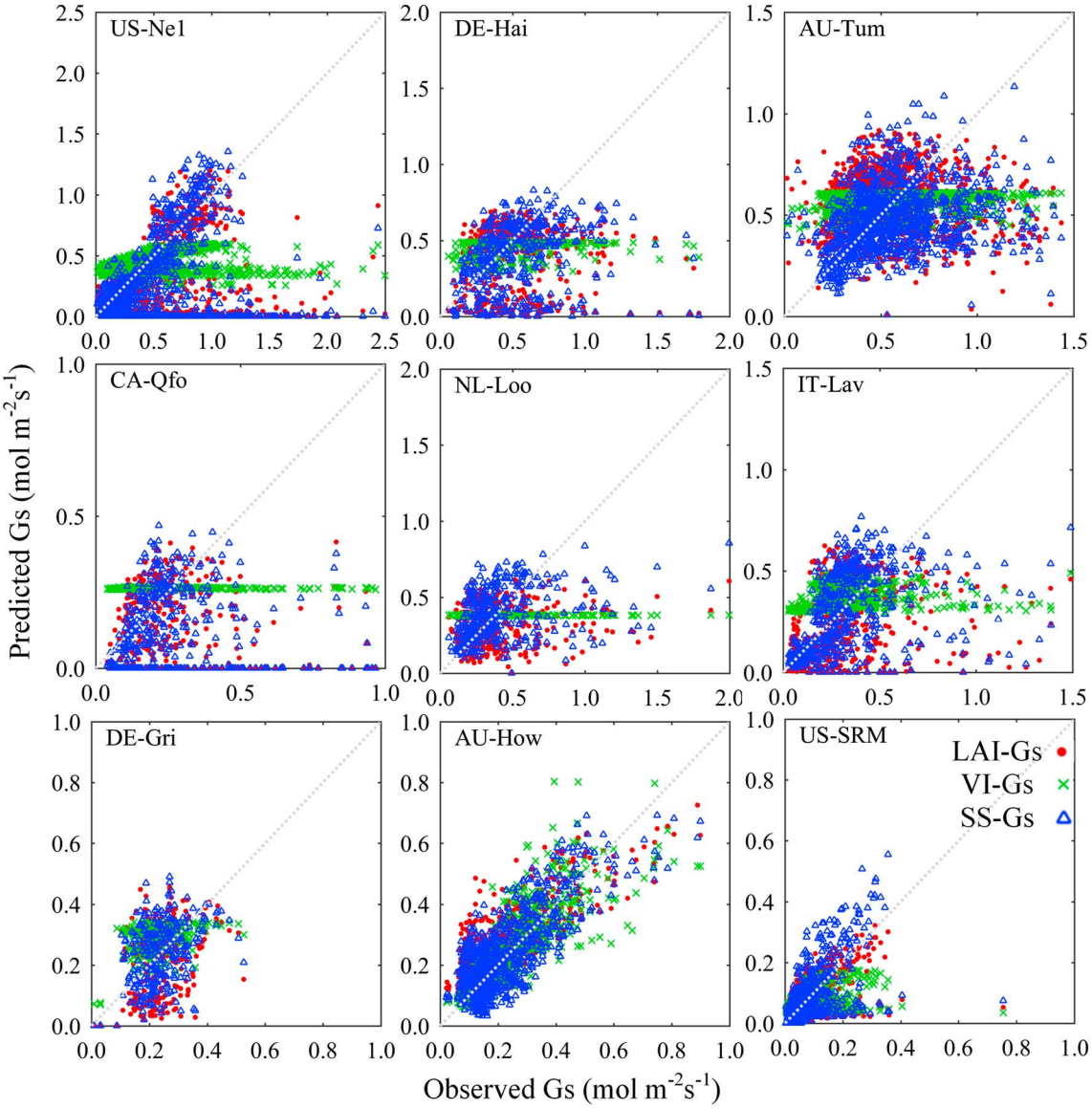

Figure 3. Comparison of the daily G_s (mol·m^{-2}·s^{-1}) estimated by three G_s models against the corresponding values derived from tower-based observations for the validation data set. Only data at nine representative sites are shown here, and for data at the remaining eight sites, see Figure S5.

model (Raich et al., 1991), the revised TL-LUE model captures the impacts of both low and high temperatures on GPP.

4.2. Ability of Different Models to Estimate Canopy Conductance and ET

Overall, the three models can be used for estimating G_s from remote sensing data, but their performances differ substantially. The LAI-G_s and VI-G_s models estimate G_s from LAI and VIs, respectively. Leaf stomata is parallelly distributed, and G_s increases with the increase of canopy coverage, which can be indicated by LAI or VIs. These two models are able to capture the overall seasonal trajectory and spatial variations of G_s. However, the VI-G_s model is unable to capture the short-term variations of the G_s caused by environmental factors, such as temperature, radiation, and VPD. And VIs are associated with both greenness and canopy coverage whose changes usually fall behind environmental factors, especially for forests (Sims et al., 2014). As to the LAI-G_s model, though containing the temperature and VPD factors, it ignores the effect of solar radiation on leaf stomata and the importance of separating sunlit and shaded leaves, resulting in uncertainties in simulated G_s and ET.

Table 7
Accuracy Metrics of Simulated ET at All Flux Sites

		LAI-ET						VI-ET						SS-ET					
		Calibration			Validation			Calibration			Validation			Calibration			Validation		
Site ID	IGBP	R^2	RMSE	AIC	R^2	RMSE	AIC	R^2	RMSE	AIC	R^2	RMSE	AIC	R^2	RMSE	AIC	R^2	RMSE	AIC
US-Ne1	CRO	0.87	0.74	2,416	0.84	0.80	2,800	0.67	1.19	3,455	0.56	1.26	3,877	0.87	0.81	2,627	0.84	0.89	3,049
US-Ne2	CRO	0.84	0.81	2,378	0.77	0.90	3,072	0.64	1.27	3,271	0.57	1.26	3,840	0.87	0.78	2,322	0.80	0.93	3,143
US-Ne3	CRO	0.87	0.67	2,113	0.87	0.69	2,372	0.74	1.05	3,035	0.71	1.07	3,370	0.88	0.69	2,159	0.87	0.75	2,553
DE-Hai	DBF	0.74	0.89	969	0.74	0.84	1,056	0.57	1.05	1,094	0.74	0.71	919	0.84	0.62	701	0.80	0.65	843
US-MMS	DBF	0.81	0.76	2,069	0.91	0.63	2,466	0.76	0.84	2,242	0.85	0.70	2,769	0.83	0.72	1,962	0.90	0.60	2,358
US-WCr	DBF	0.76	0.88	836	0.85	0.67	822	0.56	1.08	971	0.73	0.86	1,034	0.77	0.76	742	0.84	0.67	835
AU-Tum	EBF	0.76	0.96	2,754	0.79	0.99	3,245	0.74	0.89	2,618	0.75	0.99	3,249	0.77	0.72	2,197	0.77	0.72	2,516
CA-Qfo	ENF	0.80	0.50	472	0.80	0.56	641	0.71	0.64	632	0.72	0.73	848	0.85	0.39	321	0.82	0.42	432
IT-Lav	ENF	0.68	0.73	1,182	0.72	0.72	1,206	0.71	0.59	958	0.70	0.68	1,157	0.78	0.57	925	0.80	0.60	1,011
NL-Loo	ENF	0.68	0.71	749	0.61	0.95	1,037	0.56	0.93	933	0.46	0.98	1,066	0.77	0.64	682	0.73	0.79	896
US-NR1	ENF	0.71	0.85	1,220	0.71	0.88	1,307	0.66	0.68	1,007	0.67	0.67	1,036	0.75	0.60	879	0.72	0.63	980
DE-Gri	GRA	0.77	0.65	587	0.74	0.62	522	0.83	0.52	460	0.88	0.48	389	0.79	0.56	500	0.77	0.50	406
US-Var	GRA	0.31	1.02	3,084	0.35	1.01	5,378	0.52	0.85	2,694	0.59	0.81	4,540	0.58	0.62	2,028	0.61	0.61	3,473
US-Wkg	GRA	0.65	0.43	1,405	0.72	0.37	1,571	0.47	0.55	2,054	0.40	0.59	3,224	0.64	0.48	1,713	0.74	0.41	1,925
AU-How	SAV	0.70	0.68	1,414	0.57	0.82	2,013	0.81	0.51	1,015	0.82	0.47	1,102	0.57	0.77	1,584	0.48	0.83	2,025
US-SRM	WS	0.58	0.46	1,954	0.66	0.48	2,001	0.43	0.59	2,738	0.50	0.62	2,769	0.66	0.45	1,906	0.72	0.48	2,001
US-Ton	WS	0.57	0.71	1,956	0.57	0.70	3,503	0.65	0.57	1,558	0.67	0.55	2,702	0.53	0.58	1,609	0.59	0.58	2,870

Note. "LAI-ET", "VI-ET", and "SS-ET" denote ET (mm/day) simulated using the PM model along with ET-LAI, ET-VI, and ET-SS, respectively. All correlations are significant at the level of 0.01. ET = evapotranspiration; IGBP = International Geosphere-Biosphere Programme; CRO = cropland; DBF = deciduous broadleaf forest; EBF = evergreen broadleaf forest; ENF = evergreen needleleaf forest; GRA = grassland; SAV = savannas; WS = woody savannas; RMSE = root mean square error; AIC = Akaike information criterion; PM = Penman-Monteith.

Different from the LAI-G_s and VI-G_s models, the SS-G_s model estimates G_s according to the GPP of sunlit and shaded leaves, which is affected by LAI and environmental factors, including temperature, VPD, and PAR. Therefore, the impacts of LAI and environmental factors on G_s were effectively captured. Sunlit and shaded leaves have different exposure to sunlight and have different g_s, especially for forests with deep canopy. The SS-G_s model captures such difference of sunlit and shaded leaves. As a consequence, it was able to improve the estimation of G_s in growing seasons, especially at forest sites in comparison with the LAI-G_s and VI-G_s models (Figures S7 and S8).

With G_s estimated by the SS-G_s model proposed in this study, the PM model was able to improve the simulation of daily ET under most circumstances. The improvement on ET estimation was more evident in growing seasons and at forest sites (Figures S9 and S10). Both the LAI-G_s and VI-G_s models overestimated G_s at forest sites, resulting in the simulated ET being much higher than the observations. The overestimation of ET was well constrained by using G_s-SS in the PM model.

4.3. Sensitivity of ET to G_s

Tables 5–7 show that R^2 values of G_s estimation are commonly lower than those for ET estimation. For example, at the NL-Loo site, the R^2 values of estimated G_s and ET were close to 0.02 and 0.75, respectively, for the calibration data set. To explore the reason inducing such a large difference, the sensitivity of tower-based ET to parameters in the PM model was analyzed using a global sensitivity analysis method named Fourier amplitude sensitivity test (Cannavó, 2012; Saltelli et al., 1999). The global sensitivity analysis results show that G_s is the key parameter affecting ET, second only to *Rn* (Table 8). The average sensitive indices of *Rn* and G_s were 49% and 30%, respectively. The impacts of other variables on ET are relatively small. To identify whether the ET estimation could be improved by incorporating SS-G_s into the PM model, the days with G_s-SS closer to tower-based G_s than with G_s-LAI and G_s-VI were selected. Figure 6 shows that on almost 99% of these days, the estimation of ET was improved.

In order to further answer the question why the agreement between tower-based G_s and G_s-SS was much poor than the agreement between the observed ET and ET-SS (Tables 5–7), data were divided into 10 groups according to the observed ET at each site. For all groups, the ranges of observed ET are equal and statistical metrics were calculated for the difference between G_s-SS and tower-based G_s. As shown in Figure 7, large departures (red crosses) of estimated G_s from tower-based ones mostly occurred under the conditions of low ET (Figures 7 and S11). In some cases of low observed ET, tower-based G_s values were large, possibly owing to the uncertainties in calculated G_a. At the same time, estimated G_s was very low, even equal to 0, resulting from very low estimated GPP. Therefore, even if the difference between estimated and tower-based G_s was

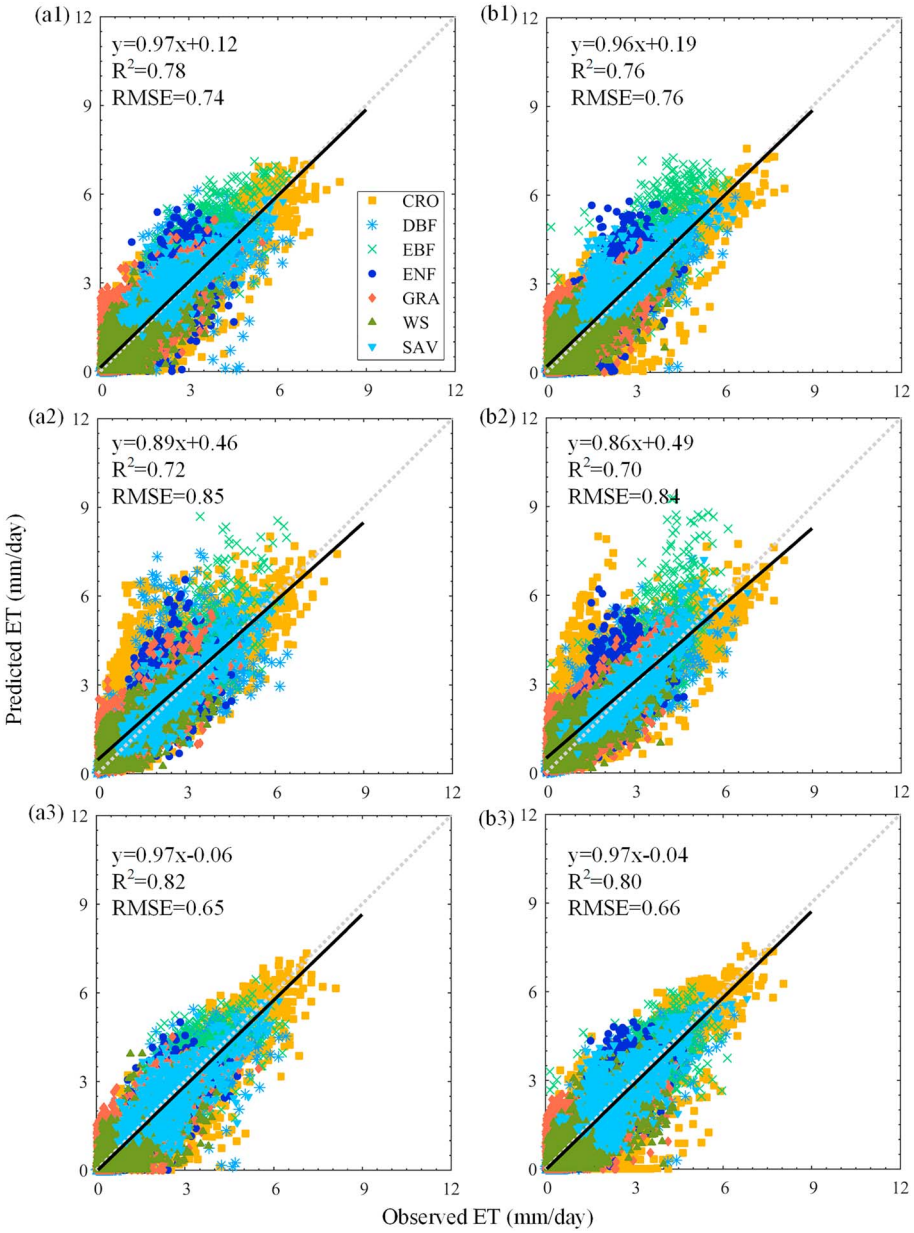

Figure 4. Comparison of the estimated daily ET (mm/day) against tower-based ET for the (a) calibration and (b) validation data sets: (a1 and b1) for ET-LAI; (a2 and b2) for ET-VI; and (a3 and b3) for ET-SS. ET = evapotranspiration; RMSE = root mean square error; CRO = cropland; DBF = deciduous broadleaf forest; EBF = evergreen broadleaf forest; ENF = evergreen needleleaf forest; GRA = grassland; SAV = savannas; WS = woody savannas.

obvious, the divergence of estimated ET from tower observation was relatively small. These situations mainly occurred in nongrowing seasons. The dismatch between low tower-observed ET and high tower-based G_s is the main reason why a poor daily conductance fit can still induce a good daily ET fit.

4.4. Limitations of the SS-G_s Model

Similar to the LAI-G_s and VI-G_s models, the SS-G_s model takes G_c as the proxy of G_s. This treatment is reasonable when the canopy coverage is high and the soil surface is dry. However, under conditions of low canopy coverage and wet soil surface, soil evaporation might account for a large proportion of ET, and G_{soil} might make a considerable contribution to G_s (Kelliher et al., 1995; Waring & Running, 2010). This limitation of the currently proposed SS-G_s model can be remedied by including a G_{soil} term or using dual-source

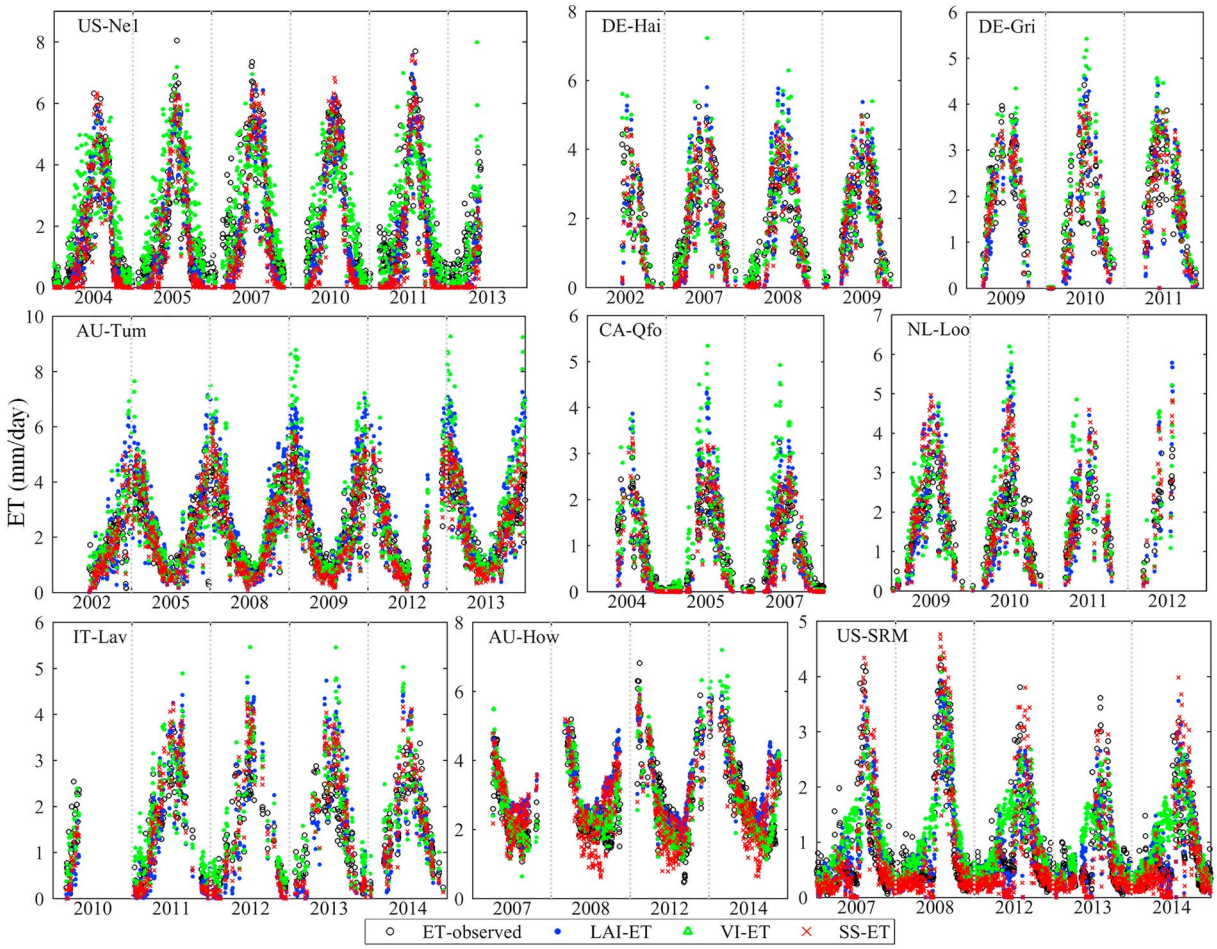

Figure 5. Daily variations of the simulated and observed evapotranspiration (ET; mm/day) for the validation data set at nine representative sites. Data for the remaining eight sites can be found in Figure S6.

Table 8
Sensitive Indices (%) of the Penman-Monteith Model for Different Input Variables at Each Site

Site ID	*T*	VPD	*Rn*	*G*	G_a	G_s
US-Ne1	2.03	0.08	53.59	1.67	0.01	28.01
US-Ne2	1.84	0.09	55.60	1.82	0.02	25.78
US-Ne3	1.75	0.09	57.88	2.02	0.02	22.84
DE-Hai	4.92	0.07	53.59	0.20	1.55	27.85
US-MMS	8.12	0.05	44.88	0.27	1.24	30.53
US-WCr	0.28	0.05	43.31	0.02	0.06	43.59
AU-Tum	3.88	0.06	49.36	0.08	1.10	34.25
CA-Qfo	11.19	0.04	38.89	0.05	0.64	34.57
IT-Lav	3.94	0.06	50.41	0.10	0.47	32.97
NL-Loo	6.00	0.08	56.07	0.06	2.08	24.28
US-NR1	1.73	0.05	40.55	0.03	0.31	45.75
DE-Gri	8.59	0.05	49.53	0.62	3.79	18.50
US-Var	6.07	0.06	55.00	0.89	1.82	24.07
US-Wkg	11.31	0.04	41.07	2.53	3.84	23.90
AU-How	2.68	0.05	45.68	0.90	4.22	37.74
US-SRM	8.15	0.05	38.32	0.98	5.18	30.38
US-Ton	4.74	0.05	53.14	0.60	2.36	25.61

models of PM to estimate evaporation and transpiration separately (Mu et al., 2007; Sun et al., 2013). Of course, G_{soil} changes with the wetness of land surface. The inclusion of this term in the SS-G_s model will require calibrating more parameters and estimating soil wetness.

The tight coupling of water and carbon cycles is the prerequisite of the SS-G_s model. Previous studies indicated that water stress might induce breakdown of carbon-water relations (Damour et al., 2010; Nelson et al., 2018). The applicability of the SS-G_s model under different conditions of water stress needs further investigation. In addition, accurately estimating GPP of sunlit and shaded leaves is the foundation of the SS-G_s model. However, parameters ε_{msh} and ε_{msu} are crucial for simulating GPP by the TL-LUE model, and they vary substantially among different vegetation types. Even within one vegetation type, their spatial and temporal variations are still large. This issue might be solved by the photochemical reflectance index, which could appropriately track the variations (Middleton et al., 2016; Zhou et al., 2017). But for the parameters g_1 and g_2 of the SS-G_s model (equation (4)), they exhibit considerable variations as indicated by the calibration outputs. How to capture the spatial variations of g_1 and g_2 is a big challenge for the SS-G_s model when applied over large regions.

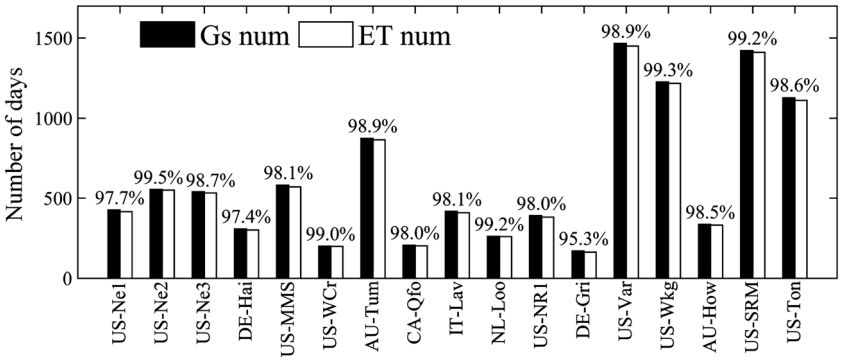

Figure 6. The number of days with G_s (mol·m^{-2}·s^{-1}) and evapotranspiration (ET; mm/day) estimates improved by the SS-G_s model at each site. "G_s num" is the number of days with G_s-SS closer to tower-based G_s than with G_s-LAI and G_s-VI. Among these days, the number of days with ET estimates improved is shown as "ET num." The percentage numbers above vertical bars represent ratios of "ET num" to the corresponding "G_s num."

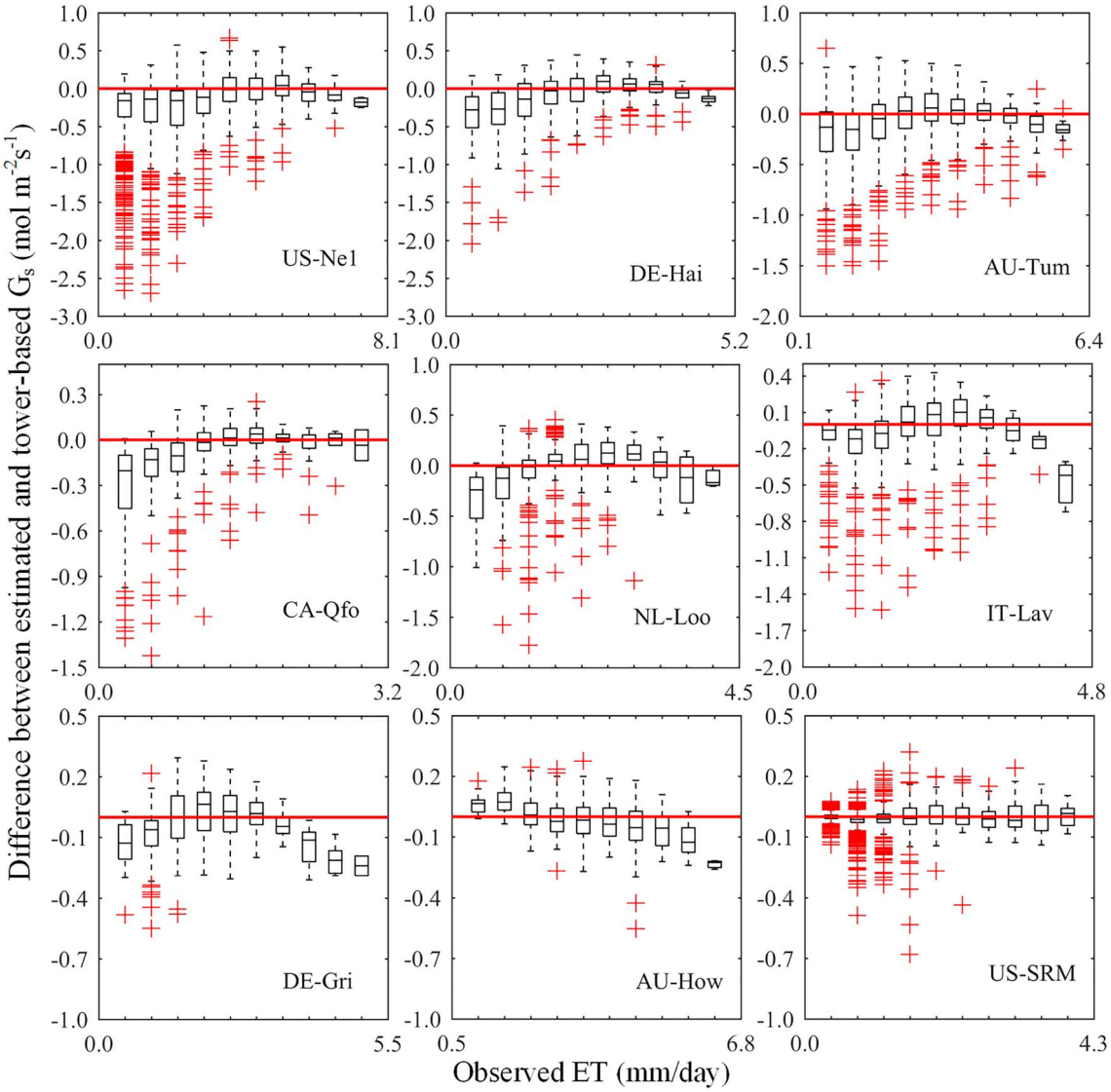

Figure 7. Difference between the estimated and tower-based G_s (mol·m^{-2}·s^{-1}) in different ranges of tower-observed evapotranspiration (ET; mm/day) at nine representative sites. The red crosses represent outliers. Negative y values mean the G_s estimates were lower than tower-based ones, and vice versa. Data for the remaining eight sites are shown in Figure S11.

It should be kept in mind there are uncertainties in the current validation process. As is known, canopy G_s is not directly measurable. In this study, G_s used for validating the LAI-G_s, VI-G_s, and SS-G_s models was inverted from tower-based latent heat flux and meteorological data using equation (2). Most variables in this equation can be calculated using classical formula or measured. However, when G_a was estimated using equation (3), it ignores the influence of the stability of atmosphere on the transfer of water vapor. This simplification might induce uncertainties in estimated G_a and consequently in G_s.

5. Conclusions

In this study, we proposed an algorithm for estimating G_s, a key parameter in the PM model. This algorithm accounts for the difference in stomatal conductance of sunlit and shade leaves in canopies and their contributions to G_s and further ET estimates. In this algorithm, the Ball-Berry model is used to link stomatal conductance of sunlit and shade leaves with their respective GPP, which is estimated using a revised TL-LUE model. We tested the algorithm with at least 6 years in situ flux data from 17 FLUXNET sites covering seven different vegetation types. Following conclusions could be drawn:

1. By accounting for the adverse impact of both low and high temperatures on GPP, the revised TL-LUE model improves GPP simulation, especially at the crop and forest sites.
2. The proposed SS-G_s model was able to estimate daily G_s well, outperforming the VI-G_s and LAI-G_s models in growing seasons, especially at the forest sites.
3. ET estimation is substantially improved with G_s estimated using the proposed SS-G_s model. ET estimated using the proposed SS-G_s model shows good agreement with tower-based ET for all vegetation types, while ET estimated using the VI-G_s and LAI-G_s models was divergent from observations for the crop and forest sites.

There are some remaining issues regarding the further examination and improvement of the proposed SS-G_s model, such as validating across more ecosystems under different conditions of canopy coverage and land surface wetness, considering spatiotemporal variations of the model parameters, and bettering the agreement between estimated G_s and observed ones under different circumstances. Nevertheless, this study explored an effective and applicable algorithm for improving G_s estimation, which is potentially applicable at regional and global scales.

Acknowledgments
This research was funded by the National Key R&D Program of China (2016YFA0600202) and the National Natural Science Foundation of China (41671343). This work used eddy covariance data acquired and shared by the FLUXNET community, including these networks: AmeriFlux, AfriFlux, AsiaFlux, CarboAfrica, CarboEuropeIP, CarboItaly, CarboMont, ChinaFlux, Fluxnet-Canada, GreenGrass, ICOS, KoFlux, LBA, NECC, OzFlux-TERN, TCOS-Siberia, and TERENO and USCCC. The FLUXNET eddy covariance data processing and harmonization was carried out by the ICOS Ecosystem Thematic Center, AmeriFlux Management Project, and Fluxdata Project of FLUXNET, with the support of CDIAC, and the OzFlux, ChinaFlux, and AsiaFlux offices. The FLUXNET data are freely available at http://fluxnet.fluxdata.org. The MODIS data are freely available at https://lpdaac.usgs.gov.

References

Allen, R. G., Pereira, L. S., Smith, M., Raes, D., & Wright, J. L. (2005). FAO-56 dual crop coefficient method for estimating evaporation from soil and application extensions. *Journal of Irrigation and Drainage Engineering*, *131*(1), 2–13. https://doi.org/10.1061/(ASCE)0733-9437(2005)131:1(2)

Baldocchi, D., Chen, Q., Chen, X., Ma, S., Miller, G., Ryu, Y., et al. (2010). The dynamics of energy, water, and carbon fluxes in a blue oak (*Quercus douglasii*) savanna in California. *Ecosystem Function in Savannas*, 135–154. https://doi.org/10.1201/b10275-10

Ball, J. T., Woodrow, I. E., & Berry, J. A. (1987). A model predicting stomatal conductance and its contribution to the control of photosynthesis under different environmental conditions. *Progress in Photosynthesis Research*, *1*, 221–224. https://doi.org/10.1007/978-94-017-0519-6_48

Bergeron, O., Margolis, H. A., Black, T. A., Coursolle, C., Dunn, A. L., Barr, A. G., & Wofsy, S. C. (2007). Comparison of carbon dioxide fluxes over three boreal black spruce forests in Canada. *Global Change Biology*, *13*(1), 89–107. https://doi.org/10.1111/j.1365-2486.2006.01281.x

Beringer, J., Hutley, L. B., Tapper, N. J., Coutts, A., Kerley, A., & O'grady, A. P. (2003). Fire impacts on surface heat, moisture and carbon fluxes from a tropical savanna in northern Australia. *International Journal of Wildland Fire*, *12*(4), 333–340. https://doi.org/10.1071/WF03023

Cannavó, F. (2012). Sensitivity analysis for volcanic source modeling quality assessment and model selection. *Computers and Geosciences*, *44*, 52–59. https://doi.org/10.1016/j.cageo.2012.03.008

Chapin, F. S., Pickett, S. T., Power, M. E., Jackson, R. B., Carter, D. M., & Duke, C. (2011). Earth stewardship: A strategy for social–ecological transformation to reverse planetary degradation. *Journal of Environmental Studies and Sciences*, *1*(1), 44–53. https://doi.org/10.1007/s13412-011-0010-7

Chen, J. M., Liu, J., Cihlar, J., & Goulden, M. L. (1999). Daily canopy photosynthesis model through temporal and spatial scaling for remote sensing applications. *Ecological Modelling*, *124*(2–3), 99–119. https://doi.org/10.1016/S0304-3800(99)00156-8

Chen, J. M., Deng, F., & Chen, M. (2006). Locally adjusted cubic-spline capping for reconstructing seasonal trajectories of a satellite-derived surface parameter. *IEEE Transactions on Geoscience and Remote Sensing*, *44*(8), 2230–2238. https://doi.org/10.1109/TGRS.2006.872089

Cleugh, H. A., Leuning, R., Mu, Q., & Running, S. W. (2007). Regional evaporation estimates from flux tower and MODIS satellite data. *Remote Sensing of Environment*, *106*(3), 285–304. https://doi.org/10.1016/j.rse.2006.07.007

Cook, B. D., Davis, K. J., Wang, W., Desai, A., Berger, B. W., Teclaw, R. M., et al. (2004). Carbon exchange and venting anomalies in an upland deciduous forest in northern Wisconsin USA. *Agricultural and Forest Meteorology*, *126*(3–4), 271–295. https://doi.org/10.1016/j.agrformet.2004.06.008

Dai, Y., Dickinson, R. E., & Wang, Y. P. (2004). A two-big-leaf model for canopy temperature, photosynthesis, and stomatal conductance. *Journal of Climate*, *17*(12), 2281–2299. https://doi.org/10.1175/1520-0442(2004)017<2281:ATMFCT>2.0.CO;2

Damour, G., Simonneau, T., Cochard, H., & Urban, L. (2010). An overview of models of stomatal conductance at the leaf level. *Plant, Cell & Environment*, *33*(9), 1419–1438. https://doi.org/10.1111/j.1365-3040.2010.02181.x

Dickinson, R. E., Oleson, K. W., Bonan, G., Hoffman, F., Thornton, P., Vertenstein, M., et al. (2006). The Community Land Model and its climate statistics as a component of the Community Climate System Model. *Journal of Climate*, *19*(11), 2302–2324. https://doi.org/10.1175/JCLI3742.1

Dolman, A. J., Moors, E. J., & Elbers, J. A. (2002). The carbon uptake of a mid latitude pine forest growing on sandy soil. *Agricultural and Forest Meteorology*, *111*(3), 157–170. https://doi.org/10.1016/S0168-1923(02)00024-2

Fiora, A., & Cescatti, A. (2006). Diurnal and seasonal variability in radial distribution of sap flux density: Implications for estimating stand transpiration. *Tree Physiology*, *26*(9), 1217–1225. https://doi.org/10.1093/treephys/26.9.1217

Glenn, E. P., Nagler, P. L., & Huete, A. R. (2010). Vegetation index methods for estimating evapotranspiration by remote sensing. *Surveys in Geophysics*, *31*(6), 531–555. https://doi.org/10.1007/s10712-010-9102-2

Glenn, E. P., Neale, C. M., Hunsaker, D. J., & Nagler, P. L. (2011). Vegetation index-based crop coefficients to estimate evapotranspiration by remote sensing in agricultural and natural ecosystems. *Hydrological Processes*, *25*(26), 4050–4062. https://doi.org/10.1002/hyp.8392

Guerschman, J. P., Van Dijk, A. I., Mattersdorf, G., Beringer, J., Hutley, L. B., Leuning, R., et al. (2009). Scaling of potential evapotranspiration with MODIS data reproduces flux observations and catchment water balance observations across Australia. *Journal of Hydrology*, *369*(1–2), 107–119. https://doi.org/10.1016/j.jhydrol.2009.02.013

Hansen, M. C., & Reed, B. (2000). A comparison of the IGBP DISCover and University of Maryland 1 km global land cover products. *International Journal of Remote Sensing*, *21*(6–7), 1365–1373. https://doi.org/10.1080/014311600210218

He, M., Ju, W., Zhou, Y., Chen, J., He, H., Wang, S., et al. (2013). Development of a two-leaf light use efficiency model for improving the calculation of terrestrial gross primary productivity. *Agricultural and Forest Meteorology*, *173*, 28–39. https://doi.org/10.1016/j.agrformet.2013.01.003

Hu, Z., Yu, G., Zhou, Y., Sun, X., Li, Y., Shi, P., et al. (2009). Partitioning of evapotranspiration and its controls in four grassland ecosystems: Application of a two-source model. *Agricultural and Forest Meteorology*, *149*(9), 1410–1420. https://doi.org/10.1016/j.agrformet.2009.03.014

Huete, A., Didan, K., Miura, T., Rodriguez, E. P., Gao, X., & Ferreira, L. G. (2002). Overview of the radiometric and biophysical performance of the MODIS vegetation indices. *Remote Sensing of Environment*, *83*(1–2), 195–213. https://doi.org/10.1016/S0034-4257(02)00096-2

Huntington, T. G. (2006). Evidence for intensification of the global water cycle: Review and synthesis. *Journal of Hydrology*, *319*(1-4), 83–95. https://doi.org/10.1016/j.jhydrol.2005.07.003

Inouye, T., Toi, S., & Matsumoto, Y. (1995). A new segmentation method of electroencephalograms by use of Akaike's information criterion. *Cognitive Brain Research*, *3*(1), 33–40. https://doi.org/10.1016/0926-6410(95)00016-X

Irmak, S., Mutiibwa, D., Irmak, A., Arkebauer, T. J., Weiss, A., Martin, D. J., & Eisenhauer, D. E. (2008). On the scaling up leaf stomatal resistance to canopy resistance using photosynthetic photon flux density. *Agricultural and Forest Meteorology*, *148*(6–7), 1034–1044. https://doi.org/10.1016/j.agrformet.2008.02.001

Jarvis, P. G. (1976). The interpretation of the variations in leaf water potential and stomatal conductance found in canopies in the field. *Philosophical Transactions of The Royal Society B Biological Sciences*, *273*(927), 593–610. https://doi.org/10.1098/rstb.1976.0035

Jun, C., Ban, Y., & Li, S. (2014). China: Open access to Earth land-cover map. *Nature*, *514*(7523), 434. https://doi.org/10.1038/514434c

Kelliher, F. M., Leuning, R., Raupach, M. R., & Schulze, E. D. (1995). Maximum conductances for evaporation from global vegetation types. *Agricultural and Forest Meteorology*, *73*(1–2), 1–16. https://doi.org/10.1016/0168-1923(94)02178-M

Knohl, A., Schulze, E. D., Kolle, O., & Buchmann, N. (2003). Large carbon uptake by an unmanaged 250-year-old deciduous forest in Central Germany. *Agricultural and Forest Meteorology*, *118*(3–4), 151–167. https://doi.org/10.1016/S0168-1923(03)00115-1

Leuning, R., Cleugh, H. A., Zegelin, S. J., & Hughes, D. (2005). Carbon and water fluxes over a temperate Eucalyptus forest and a tropical wet/dry savanna in Australia: Measurements and comparison with MODIS remote sensing estimates. *Agricultural and Forest Meteorology*, *129*(3–4), 151–173. https://doi.org/10.1016/j.agrformet.2004.12.004

Leuning, R., Zhang, Y. Q., Rajaud, A., Cleugh, H., & Tu, K. (2008). A simple surface conductance model to estimate regional evaporation using MODIS leaf area index and the Penman-Monteith equation. *Water Resources Research*, *44*, W10419. https://doi.org/10.1029/2007WR006562

Liang, S. (2001). Narrowband to broadband conversions of land surface albedo I: Algorithms. *Remote Sensing of Environment*, *76*(2), 213–238. https://doi.org/10.1016/S0034-4257(00)00205-4

Luo, X., Croft, H., Chen, J. M., Bartlett, P., Staebler, R., & Froelich, N. (2018). Incorporating leaf chlorophyll content into a two-leaf terrestrial biosphere model for estimating carbon and water fluxes at a forest site. *Agricultural and Forest Meteorology*, *248*, 156–168. https://doi.org/10.1016/j.agrformet.2017.09.012

L'vovich, M. I., White, G. F., Belyaev, A. V., Kindler, J., Koronkevic, N. I., Lee, T. R., & Voropaev, G. V. (1990). *Use and transformation of terrestrial water systems. The Earth as transformed by human action global and regional changes in the biosphere over the past 300 years*, (pp. 235–252). CA: Cambridge: Cambridge University Press.

Ma, S., Baldocchi, D. D., Xu, L., & Hehn, T. (2007). Inter-annual variability in carbon dioxide exchange of an oak/grass savanna and open grassland in California. *Agricultural and Forest Meteorology*, *147*(3–4), 157–171. https://doi.org/10.1016/j.agrformet.2007.07.008

Marshall, M., Thenkabail, P., Biggs, T., & Post, K. (2016). Hyperspectral narrowband and multispectral broadband indices for remote sensing of crop evapotranspiration and its components (transpiration and soil evaporation). *Agricultural and Forest Meteorology*, *218*, 122–134. https://doi.org/10.1016/j.agrformet.2015.12.025

Middleton, E. M., Huemmrich, K. F., Cheng, Y. B., & Margolis, H. A. (2016). 12 spectral bioindicators of photosynthetic efficiency and vegetation stress. *Hyperspectral remote sensing of vegetation*, *265*. https://doi.org/10.1201/b11222-18

Moffat, A. M., Papale, D., Reichstein, M., Hollinger, D. Y., Richardson, A. D., Barr, A. G., et al. (2007). Comprehensive comparison of gap-filling techniques for eddy covariance net carbon fluxes. *Agricultural and Forest Meteorology*, *147*(3–4), 209–232. https://doi.org/10.1016/j.agrformet.2007.08.011

Monson, R. K., Turnipseed, A. A., Sparks, J. P., Harley, P. C., Scott-Denton, L. E., Sparks, K., & Huxman, T. E. (2002). Carbon sequestration in a high-elevation, subalpine forest. *Global Change Biology*, *8*(5), 459–478. https://doi.org/10.1046/j.1365-2486.2002.00480.x

Monteith, J., & Unsworth, M. (2013). *Principles of environmental physics: Plants, animals, and the atmosphere* (4th ed.). CA: Academic Press.

Monteith, J. L. (1965). *Evaporation and environment*. Symposia of the Society for Experimental Biology. CA: Cambridge: Cambridge University Press.

Mu, Q., Heinsch, F. A., Zhao, M., & Running, S. W. (2007). Development of a global evapotranspiration algorithm based on MODIS and global meteorology data. *Remote Sensing of Environment*, *111*(4), 519–536. https://doi.org/10.1016/j.rse.2007.04.015

Nelson, J. A., Carvalhais, N., Migliavacca, M., Reichstein, M., & Jung, M. (2018). Water-stress-induced breakdown of carbon–water relations: Indicators from diurnal FLUXNET patterns. *Biogeosciences*, *15*(8), 2433–2447. https://doi.org/10.5194/bg-15-2433-2018

Newman, B. D., Wilcox, B. P., Archer, S. R., Breshears, D. D., Dahm, C. N., Duffy, C. J., et al. (2006). Ecohydrology of water-limited environments: A scientific vision. *Water Resources Research*, *42*, W06302. https://doi.org/10.1029/2005WR004141

Norman, J. M. (1980). Interfacing leaf and canopy light interception models. *Photosynthesis for Ecosystem Models*, *2*, 49–67.

Papale, D., Reichstein, M., Aubinet, M., Canfora, E., Bernhofer, C., Kutsch, W., et al. (2006). Towards a standardized processing of net ecosystem exchange measured with eddy covariance technique: Algorithms and uncertainty estimation. *Biogeosciences*, *3*(4), 571–583. https://doi.org/10.5194/bg-3-571-2006

Prescher, A. K., Grünwald, T., & Bernhofer, C. (2010). Land use regulates carbon budgets in eastern Germany: From NEE to NBP. *Agricultural and Forest Meteorology*, *150*(7–8), 1016–1025. https://doi.org/10.1016/j.agrformet.2010.03.008

Raich, J. W., Rastetter, E. B., Melillo, J. M., Kicklighter, D. W., Steudler, P. A., Peterson, B. J., et al. (1991). Potential net primary productivity in South America: Application of a global model. *Ecological Applications*, *1*(4), 399–429. https://doi.org/10.2307/1941899

Rouse, J. W. Jr., Haas, R. H., Schell, J. A., & Deering, D. W. (1973). *Monitoring the vernal advancement and retrogradation (green wave effect) of natural vegetation*. Greenbelt, MD: NASA/GSFC Type III. Final Report

Running, S. W., Thornton, P. E., Nemani, R., & Glassy, J. M. (2000). Global terrestrial gross and net primary productivity from the Earth Observing System. *Methods in ecosystem science*, 44–57. https://doi.org/10.1007/978-1-4612-1224-9_4

Saltelli, A., Tarantola, S., & Chan, K. S. (1999). A quantitative model-independent method for global sensitivity analysis of model output. *Technometrics*, *41*(1), 39–56. https://doi.org/10.1080/00401706.1999.10485594

Schmid, H. P., Grimmond, C. S. B., Cropley, F., Offerle, B., & Su, H. B. (2000). Measurements of CO2 and energy fluxes over a mixed hardwood forest in the mid-western United States. *Agricultural and Forest Meteorology*, *103*(4), 357–374. https://doi.org/10.1016/S0168-1923(00)00140-4

Scott, R. L. (2010). Using watershed water balance to evaluate the accuracy of eddy covariance evaporation measurements for three semiarid ecosystems. *Agricultural and Forest Meteorology*, *150*(2), 219–225. https://doi.org/10.1016/j.agrformet.2009.11.002

Scott, R. L., Jenerette, G. D., Potts, D. L., & Huxman, T. E. (2009). Effects of seasonal drought on net carbon dioxide exchange from a woody-plant-encroached semiarid grassland. *Journal of Geophysical Research*, *114*, G04004. https://doi.org/10.1029/2008JG000900

Senay, G., Budde, M., Verdin, J., & Melesse, A. (2007). A coupled remote sensing and simplified surface energy balance approach to estimate actual evapotranspiration from irrigated fields. *Sensors*, *7*(6), 979–1000. https://doi.org/10.3390/s7060979

Sims, D. A., Brzostek, E. R., Rahman, A. F., Dragoni, D., & Phillips, R. P. (2014). An improved approach for remotely sensing water stress impacts on forest C uptake. *Global Change Biology*, *20*(9), 2856–2866. https://doi.org/10.1111/gcb.12537

Sinclair, T. R., Murphy, C. E., & Knoerr, K. R. (1976). Development and evaluation of simplified models for simulating canopy photosynthesis and transpiration. *Journal of Applied Ecology*, *13*(3), 813–829. https://doi.org/10.2307/2402257

Sun, L., Liang, S., Yuan, W., & Chen, Z. (2013). Improving a Penman–Monteith evapotranspiration model by incorporating soil moisture control on soil evaporation in semiarid areas. *International Journal of Digital Earth*, *6*(sup1), 134–156. https://doi.org/10.1080/17538947.2013.783635

Teuling, A. J., Uijlenhoet, R., van den Hurk, B., & Seneviratne, S. I. (2009). Parameter sensitivity in LSMs: An analysis using stochastic soil moisture models and ELDAS soil parameters. *Journal of Hydrometeorology*, *10*(3), 751–765. https://doi.org/10.1175/2008JHM1033.1

Verma, S. B., Dobermann, A., Cassman, K. G., Walters, D. T., Knops, J. M., Arkebauer, T. J., et al. (2005). Annual carbon dioxide exchange in irrigated and rainfed maize-based agroecosystems. *Agricultural and Forest Meteorology*, *131*(1–2), 77–96. https://doi.org/10.1016/j.agrformet.2005.05.003

Wang, J., Xiao, X., Wagle, P., Ma, S., Baldocchi, D., Carrara, A., et al. (2016). Canopy and climate controls of gross primary production of Mediterranean-type deciduous and evergreen oak savannas. *Agricultural and Forest Meteorology*, *226-227*, 132–147. https://doi.org/10.1016/j.agrformet.2016.05.020

Waring, R. H., & Running, S. W. (2010). *Forest ecosystems: analysis at multiple scales*, (Vol. 420). London: Elsevier.

Went, F. W. (1953). The effect of temperature on plant growth. *Annual Review of Plant Physiology*, *4*(1), 347–362. https://doi.org/10.1146/annurev.pp.04.060153.002023

Whitehead, D., Okali, D. U. U., & Fasehun, F. E. (1981). Stomatal response to environmental variables in two tropical forest species during the dry season in Nigeria. *Journal of Applied Ecology*, *18*(2), 571–587. https://doi.org/10.2307/2402418

Wu, G., Hu, Z., Li, S., Zheng, H., Zhu, X., Sun, X., et al. (2016). Evaluation and uncertainty analysis of a two-source evapotranspiration model. *Acta Geographica Sinica*, *71*(11), 1886–1897. https://doi.org/10.11821/dlxb201611002

Xin, X. Z., Tian, G. L., & Liu, Q. H. (2003). A review of researches on remote sensing of land surface evapotranspiration. *Journal of Remote Sensing*, *7*(3), 231–240. https://doi.org/1007-4619(2003)03-0233-08

Yebra, M., Van Dijk, A., Leuning, R., Huete, A., & Guerschman, J. P. (2013). Evaluation of optical remote sensing to estimate actual evapotranspiration and canopy conductance. *Remote Sensing of Environment*, *129*, 250–261. https://doi.org/10.1016/j.rse.2012.11.004

Zhang, B., Liu, Y., Xu, D., Cai, J., & Li, F. (2011). Evapotranspiraton estimation based on scaling up from leaf stomatal conductance to canopy conductance. *Agricultural and Forest Meteorology*, *151*(8), 1086–1095. https://doi.org/10.1016/j.agrformet.2011.03.012

Zhou, Y., Hilker, T., Ju, W., Coops, N. C., Black, T. A., Chen, J. M., & Wu, X. (2017). Modeling gross primary production for sunlit and shaded canopies across an evergreen and a deciduous site in Canada. *IEEE Transactions on Geoscience and Remote Sensing*, *55*(4), 1859–1873. https://doi.org/10.1109/TGRS.2016.2615102

Zhou, Y., Wu, X., Ju, W., Chen, J. M., Wang, S., Wang, H., et al. (2016). Global parameterization and validation of a two-leaf light use efficiency model for predicting gross primary production across FLUXNET sites. *Journal of Geophysical Research: Biogeosciences*, *121*, 1045–1072. https://doi.org/10.1002/2014JG002876